

Spin-polarized two-dimensional electron/hole gas at the interface of non-magnetic semiconducting half-Heusler compounds: Modified Slater-Pauling rule for half-metallicity at the interface

Emel Gürbüz¹, Sukanya Ghosh¹, Ersoy Şaşıoğlu^{2,*}, Iosif Galanakis^{3,†}, Ingrid Mertig², and Biplab Sanyal^{1,‡}

¹*Department of Physics and Astronomy, Uppsala University, 75120 Uppsala, Sweden*

²*Institute of Physics, Martin Luther University Halle-Wittenberg, 06120 Halle (Saale), Germany*

³*Department of Materials Science, School of Natural Sciences, University of Patras, GR-26504 Patra, Greece*

(Dated: February 10, 2023)

Half-Heusler compounds with 18 valence electrons per unit cell are well-known non-magnetic semiconductors. Employing first-principles electronic band structure calculations, we study the interface properties of the half-Heusler heterojunctions based on FeVSb, CoTiSb, CoVSn, and NiTiSn compounds, which belong to this category of materials. Our results show that several of these heterojunction interfaces become not only metallic but also magnetic. The emergence of spin-polarization is accompanied by the formation of two-dimensional electron gas (2DEG) or hole gas (2DHG) at the interface. We qualitatively discuss the origin of the spin polarization at the interfaces on the basis of the Stoner model. For the cases of magnetic interfaces where half-metallicity is also present, we propose a modified Slater-Pauling rule similar to the one for bulk half-metallic half-Heusler compounds. Additionally, we calculate exchange parameters, Curie temperatures and magnetic anisotropy energies for magnetic interfaces. Our study, combined with the recent experimental evidence for the presence of 2DEG at CoTiSb/NiTiSn heterojunctions might motivate future efforts and studies toward the experimental realization of devices using the proposed heterojunctions.

I. INTRODUCTION

Heusler compounds, named after Fritz Heusler [1, 2], are ternary and quaternary intermetallic compounds that crystallize in close-packed lattice structures [3–5]. Especially, the discovery of half-metallicity (the electronic band structure is metallic for one spin channel and semiconducting for the other [6]) in Heusler compounds, which was followed by other exotic behaviors like spin-gapless semiconductors and spin-filter materials [7], led to the proposal of novel devices [8–12]. An important role in the rapid growth of this research field was played by the first-principles electronic band structure calculations. On one hand, they successfully explained the origin of half-metallicity and linked it to the magnetic properties through the so-called Slater-Pauling rules [13–18], and on the other hand, extended databases built using such calculations resulted in the prediction of hundreds of new Heusler compounds which were later grown experimentally [19–26].

Heusler compounds are categorized into various families depending on the number of atoms in the unit cell and their ordering [3, 4]. The ones having the chemical formula XYZ, where X and Y are transition-metal atoms and Z is a metalloid is named half-Heusler (or semi-Heusler compounds). When the number of valence electrons in the unit cell exceeds 19 and goes up to 22, most of them are half-metals [13]. As shown by Galanakis *et al.* the half-metallicity is directly connected to the total spin magnetic moment through the Slater Pauling rule

$M_t = Z_t - 18$, where M_t is the total spin magnetic moment in the unit cell expressed in μ_B and Z_t is the total number of valence electrons in the unit cell. The number 18 expresses the fact that there are exactly nine occupied states in the minority-spin electronic band structure, which exhibits semiconducting behavior. There is a single s and a triple p band low in energy stemming from the Z atom. The d valence orbitals of the X and Y atoms hybridize creating five occupied bonding orbitals, which are separated by an energy gap from the five unoccupied antibonding orbitals.

The Slater-Pauling rule correctly predicts that half-Heusler compounds with exactly 18 valence electrons should be non-magnetic semiconductors with a gap in both spin-channels [13]. This “18-electron rule” for semiconducting half-Heusler compounds was also derived by Jung *et al.* based on ionic arguments [27]. Among the 18-valence electron half-Heusler compounds, CoTiSb, NiTiSn, FeVSb, and CoVSn have attracted most of the attention. Pierre and collaborators in 1994 have confirmed experimentally the non-magnetic semiconducting character of NiTiSn [28]. Tobola *et al.* have shown experimentally that CoTiSb is also a non-magnetic semiconductor [29]. The experimental findings for both NiTiSn and CoTiSb have been also confirmed by ab-initio calculations in Ref. [29]. Recently, Ouardi *et al.* have synthesized CoTiSb and investigated it both theoretically and experimentally [30]. Lue and collaborators grew samples of CoVSn and their findings were consistent with a non-magnetic semiconducting behavior [31]. Finally, Mokhtari and collaborators have shown theoretically that FeVSb is also a non-magnetic semiconductor [32] followed by the experimental observation in 2020 by Shourov *et al.* [33]. Ma *et al.* in 2017 studied using first-principles calculations a total of 378 half-Heusler compounds [19].

* ersoy.sasioglu@physik.uni-halle.de

† galanakis@upatras.gr

‡ biplab.sanyal@physics.uu.se

Among them, there were 27 compounds with 18 valence electrons, including the aforementioned ones, which were all found to be non-magnetic semiconductors [19]. Doping these compounds with transition-metal atoms [34–42] or vacancies [43] leads to a half-metallic behavior.

Recently, Sharan *et al.* have studied employing *ab-initio* calculations the formation of a two-dimensional electron gas (2DEG) or hole gas (2DHG) at the interface between CoTiSb and NiTiSn compounds [44]. To model the heterojunction, they assumed a superlattice along the [001] direction. Along the [001] direction, CoTiSb is non-polar and NiTiSn is polar [44]. Similarly to the complex oxides’ polar/non-polar interfaces [45–47], a 2DEG is formed at the (TiSb)-Ni interface while a 2DHG is formed at the Co-(TiSn) interface [44]. A 2DEG(2DHG) is a type of electronic system in which a large number of electrons (holes) are confined to a very thin, two-dimensional layer like the one occurring at an interface of a heterojunction. Electrons (holes) are free to move in the two dimensions, but are strongly confined in the third dimension leading to many potential applications, including high-speed electronic devices and quantum computers [48]. The 2DEG should not be confused with the 2D electron liquid observed at surfaces of bulk semiconducting Heusler compounds [49]. Experimentally, Harrington has grown heterostructures made up of alternating 25nm thick CoTiSb and NiTiSn [50]. Although the structure of the interface has not been studied, interface transport measurements suggest that 2DEG is present at the interface giving indirect evidence for its formation [50].

The goal of this study is to provide a comprehensive understanding of the electronic and magnetic properties of interfaces formed by various combinations of CoTiSb, NiTiSn, FeVSb, and CoVSb non-magnetic semiconducting Heusler compounds along the [001] growth direction by employing state-of-the-art first-principles electronic band structure calculations. We find that for all heterojunctions except for CoTiSb/CoVSb, the emergence of 2DEG or 2DHG at the interfaces is accompanied by the occurrence of magnetism. We qualitatively discuss the origin of interface magnetism on the basis of the Stoner model. In some cases, our calculations suggest that also half-metallicity is present and we formulate a modified version of the Slater-Pauling rule to connect the magnetic properties to half-metallicity and the total number of valence electrons at the specific interface. Finally, we present the exchange constants for the magnetic interfaces and use them to predict the Curie temperature, which is important for applications. We should mention at this point that according to the Mermin-Wagner theorem, the long-range magnetic order does not exist in one- (1D) or two-dimensional (2D) isotropic magnets. But as shown recently in Ref. [51] short-range exchange interactions even in the absence of magnetic anisotropy can induce magnetic order in finite-size 2D magnets even for samples of millimeters size. Thus, the magnetic interfaces discussed in the present study are feasible and

can be realized in realistic spintronic devices. The rest of the manuscript is organized as follows: In Section II we present details of our calculations, in Section III we present our results, and finally, in Section IV we summarize our results and present the conclusions of our study.

II. COMPUTATIONAL METHOD

The bulk half-Heusler compounds XYZ crystallize in the cubic $C1_b$ lattice structures shown in the left panel of Fig. 1(a). The space group is the $F\bar{4}3m$ and actually consists of four interpenetrating f.c.c. sublattices; one is empty and the other three are occupied by the X, Y, and Z atoms. The unit cell is an f.c.c. one with three atoms as a basis along the long diagonal of the cube: X at (0 0 0), Y at $(\frac{1}{4} \frac{1}{4} \frac{1}{4})$ and Z at $(\frac{3}{4} \frac{3}{4} \frac{3}{4})$ in Wyckoff coordinates. When we consider a superlattice along the [001] direction then the consecutive layers are made up of pure X and mixed YZ layers and the in-plane unit cell is a square with lattice parameter the $\frac{1}{\sqrt{2}}$ of the cube’s lattice parameter as shown in the right panel of Fig. 1(a). For all four compounds FeVSb, CoTiSb, CoVSb, and NiTiSn we adopted the equilibrium lattice parameters calculated in Ref. [19] using the Vienna Ab-initio Simulation Package (VASP) [52, 53] in conjunction with the generalized gradient approximation (GGA) to the exchange-correlation potential [54]. We present the lattice parameters of the bulk compounds adopted in our study in Table I.

To carry out the spin-polarized density functional theory (DFT) calculations we employ the QUANTUMATK software package [55, 56]. We use linear combinations of atomic orbitals (LCAO) as a basis set together with norm-conserving PseudoDojo pseudopotentials [57] with the Perdew-Burke-Ernzerhof (PBE) parametrization of the GGA functional [54]. For the determination of the ground-state properties of the bulk compounds, we use a $15 \times 15 \times 15$ Monkhorst-Pack \mathbf{k} -point grid, while for periodic supercell calculations a $20 \times 20 \times 2$ Monkhorst-Pack \mathbf{k} -point grid is adopted [58].

When we form heterojunctions using FeVSb, CoTiSb, CoVSb, and NiTiSn compounds, we get six possible combinations and for each combination, there are two possible interface terminations denoted as Termination-1 and Termination-2 in Table III and shown in Fig. 1 using the FeVSb/CoTiSb as an example (the two possible interfaces are made up of Fe-TiSb and VSb-Co layers respectively). If one of the two interface terminations generates a 2DEG the other will be 2DHG as we will discuss when we present our results. To simulate the heterojunction we assume a supercell consisting of 29 (27) layers of FeVSb and 27 (29) layers of CoTiSb for the first (second) termination. To construct the supercell, we fix for the first material, for instance in FeVSb/CoTiSb supercell, the lattice parameter of FeVSb to be the cubic one shown in Table I. For the second compound, CoTiSb in our example, we consider an in-plane lattice parameter the one of FeVSb and we relax the out-of-plane lattice parameter

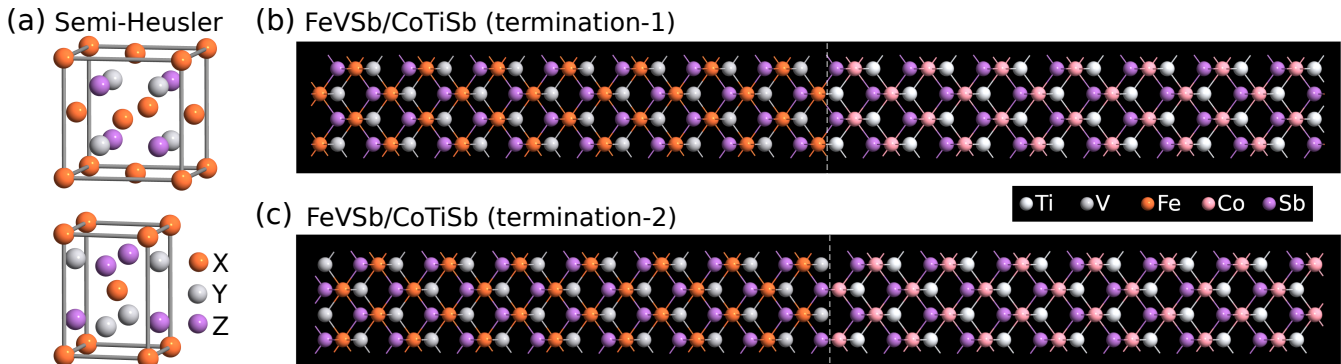


FIG. 1. (a) (Color online) Upper: Schematic representation of the conventional unit cell of XYZ half-Heusler compounds. Lower: Minimal tetragonal unit cell for the superlattice calculations (see text for details). (b) and (c) the structure of the superlattice for the two different possible interface terminations in the case of FeVSb/CoTiSb heterojunction.

along the [001] direction; in Table II we present the c/a ratio for the second compound of the heterostructure in the supercell.

In the present study, we adopted the supercell approach instead of a two-terminal device model implemented in QuantumATK and adopted in previous studies [8, 9, 11, 12] since the band structure calculations using the device model are computationally extremely demanding. For FeVSb/NiTiSn heterojunction, we performed also calculations using the device model with two semi-infinite leads by employing the nonequilibrium Green's function (NEGF) approach combined with DFT. For these DFT+NEGF calculations, we used a $20 \times 20 \times 115$ \mathbf{k} -point mesh. The results were identical to the ones obtained by the supercell approach and thus the use of the latter is completely justified.

To study finite-temperature properties of the interfaces we map the complex multi-sublattice itinerant electron problem onto a classical effective Heisenberg Hamiltonian

$$H_{\text{eff}} = - \sum_{i,j} \sum_{\mu,\nu} J_{ij}^{\mu\nu} \mathbf{S}_i^\mu \cdot \mathbf{S}_j^\nu, \quad (1)$$

where μ and ν denote different sublattices at the interface, i and j indicate atomic positions, and \mathbf{S}_i^μ is the unit vector of the i site in the μ sublattice. The Heisenberg exchange constants $J_{ij}^{\mu\nu}$ are calculated by employing the Liechtenstein formalism [59] within the full-potential linear muffin-tin orbital (FP-LMTO) code RSPt [60]. The crystalline structure information for the studied interfaces obtained with the LCAO is used as input for the electronic structure calculations by the FP-LMTO approach. According to our tests, both QuantumATK and FP-LMTO methods provide a very similar electronic structure for the systems under study. Note that in the calculation of exchange parameters, we take into account atoms at the two interface layers and the two sub-interface layers only.

To estimate the Curie temperature T_C of the magnetic interfaces, we use the mean-field approximation for

a multi-sublattice system [61–63], which is given by

$$T_C = \frac{2}{3k_B} J_L^{\mu\nu}, \quad (2)$$

where $J_L^{\mu\nu}$ is the largest eigenvalue of $J_0^{\mu\nu} = \sum_j J_{0j}^{\mu\nu}$.

III. RESULTS AND DISCUSSION

Prior to presenting our results, we should comment on our choice to use PBE which is a GGA functional in our study. GGA functionals are well-known to underestimate the band gap of semiconductors and to this respect, more elaborated functionals like the hybrid ones, which are much more demanding in computer sources, have been developed. The latter are semi-empirical combining the exact Hartree-Fock exchange with GGA and accurately reproducing the energy band gaps in usual semiconductors [64]. In Ref. [44], authors employed such a hybrid functional; the so-called Heyd, Scuseria, and Ernzerhof hybrid functional (HSE06) [65, 66] as implemented in the VASP code [52, 53]. They calculated for NiTiSn an energy band gap of 0.65 eV and for CoTiSb a value of 1.45 eV. These values are considerably larger than the 0.44 eV and 1.06 eV, respectively, calculated using PBE in Ref. [19] (as we will later discuss our PBE values are in excellent agreement with these values although we used a different electronic structure code). But, Sharon and collaborators have ignored that Heusler compounds like CoTiSb and NiTiSn are not usual semiconductors since they contain transition metal atoms and thus the accuracy of the semi-empirical hybrid functionals is not granted.

To clarify the above point we have to compare the above *ab-initio* calculations with experimental results. In Ref. [30] Ouardi and collaborators have determined the energy band gap of CoTiSb both experimentally as well as using *ab-initio* calculations employing the PBE functional. Their calculations have shown that CoTiSb exhibits an indirect gap of 1.06 eV, identical to the PBE-derived value in Ref. [19], in excellent agreement with

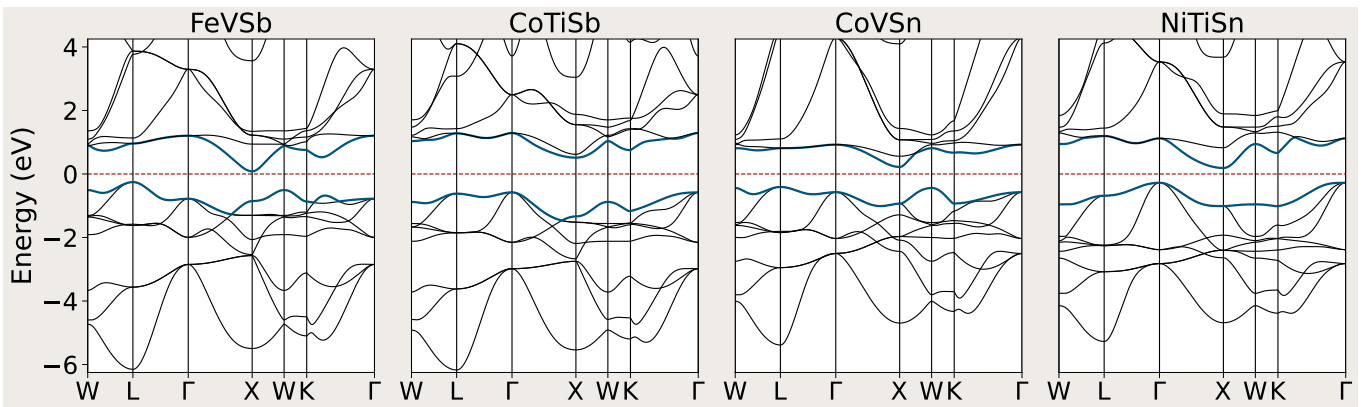


FIG. 2. (Color online) Band structure of the bulk FeVSb, CoTiSb, CoVSn, and NiTiSn half-Heusler compounds along the high-symmetry lines in the Brillouin zone. With blue we denote the topmost valence and lowest conduction bands. The Fermi level is set to zero energy.

their experimental value of about 1.0 eV. Moreover, calculations produced an optical gap (direct gap at the Γ point) of 1.83 eV also in perfect agreement with the experimental value of 1.8 eV. Finally, the experimentally determined lattice constant was 5.884 Å in perfect agreement with their own PBE calculations as well as the PBE calculations in Ref. [19]. Thus, one can safely conclude that the PBE functional is the appropriate one to study semiconductors like the half-Heusler compounds under study and the semi-empirical hybrid functionals overestimate the band gap in these materials. Moreover, as was shown in the case of transition-metal-based full-Heusler semiconductors, many-body correlations calculated using the GW approximation has minimal effect on the PBE calculated electronic band structure and the energy gaps increase by less than 0.2 eV in all cases [67]. We should finally note that, as shown in Ref. [68], the use of the more elaborated meta-GGA functionals for semiconductors lead to energy gaps that are less accurate with respect to the PBE calculated ones when compared to experimental data. .

A. Electronic structure of bulk semiconducting half-Heusler compounds

The starting point of our study is the calculation of the electronic properties of bulk materials. As mentioned above for all four compounds FeVSb, CoTiSb, CoVSn, and NiTiSn, we have adopted the equilibrium lattice constants calculated in Ref. [19] and we present them in Table I together with the band gap values. All four compounds were found to be non-magnetic semiconductors in agreement with previous first-principles calculations [19, 28, 29, 31, 32] and in Fig. 2 we present the calculated electronic band structure along the high-symmetry directions in the Brillouin zone. As the band structure plots reveal, they are indirect band-gap semiconductors but the valence band maximum (VBM) and the conduc-

tion band minimum (CBM) do not occur at the same high-symmetry points for all compounds. The character of the bands follows the discussion on the minority-spin band structure in half-Heusler compounds [13]. There are exactly nine occupied bands below the Fermi level and each band accommodates two electrons due to the spin-degeneracy. The lowest band, not-shown in Fig. 2 stems from the s states of the Sn(Sb) atoms. The lowest shown bands, which are triply degenerate at the Γ point come from the valence p bands of the Sn(Sb) atoms. Afterward, there are two almost flat bands, which are degenerate at the Γ point and stem from the bonding d states between the transition metal atoms. These bonding orbitals are of e_g character. Just below the Fermi level, the bands are triply degenerate at the Γ point and stem from the bonding t_{2g} orbitals between the neighboring transition metal atoms. These last are separated with a gap from the antibonding d states stemming from the hybridization between the d states of the transition-metal atoms.

In Table I, we also present the calculated band gap E_{gap} values, in eV units. The calculated values are in ascending order 0.34, 0.47, 0.63, and 1.09 eV for FeVSb, NiTiSb, CoVSn, and CoTiSb respectively. These values are very close to the ones calculated for the same lattice

TABLE I. Equilibrium lattice parameters (a) taken from Ref.[19], number of valence electrons per unit cell (Z_t), band gap E_g , position of the valence band maximum (E_{VB}) and of the conduction band minimum (E_{CB}) with respect to the Fermi level for FeVSb, CoTiSb, CoVSn, and NiTiSn half-Heusler compounds.

Compound	a(Å)	Z_t	E_g (eV)	E_{VB} (eV)	E_{CB} (eV)
FeVSb	5.78	18	0.34	-0.26	0.08
CoTiSb	5.88	18	1.09	-0.58	0.51
CoVSn	5.79	18	0.63	-0.41	0.22
NiTiSn	5.93	18	0.47	-0.28	0.19

TABLE II. Six possible half-Heusler heterojunctions made up of the four considered compounds. The c/a ratios are provided for the second half-Heusler compound in the heterojunction. For the two layers at each interface, we provide the calculated atomic and total spin magnetic moments as well as the ideal value for half-metallicity predicted by the $M_t^{\text{SP}} = \frac{Z_t}{2} - 9$ Slater-Pauling rule. The last column describes the character of each interface termination with respect to the 2-dimensional electron gas (2DEG). SPHG stands for spin-polarized hole gas, HG for hole gas, SPEG for spin-polarized electron gas, and EG for electron gas.

Half-Heusler Heterojunction	c/a	Termination-1						Termination-2							
		Composition	Z_t	M_X	M_Y	M_t	M_t^{SP}	2DEG	Composition	Z_t	M_X	M_Y	M_t	M_t^{SP}	2DEG
FeVSb/CoTiSb	1.03	Fe TiSb	17	-0.49	0.08	-0.42	-0.5	SPHG	VSb Co	19	-0.10	0.76	0.64	0.5	SPEG
FeVSb/CoVSn	1.01	Fe VSn	17	-0.81	0.29	-0.54	-0.5	SPHG	VSb Co	19	-0.03	0.18	0.15	0.5	SPEG
FeVSb/NiTiSn	1.05	Fe TiSn	16	-1.12	0.17	-0.99	-1.0	SPHG	VSb Ni	20	0.01	1.26	1.23	1.0	SPEG
CoTiSb/CoVSn	0.98	Co VSn	18	0.00	0.00	0.00	0.0		TiSb Co	18	0.00	0.00	0.00	0.0	
CoTiSb/NiTiSn	1.02	Co TiSn	17	0.00	0.00	0.00	-0.5	HG	TiSb Ni	19	0.00	0.00	0.00	0.5	EG
CoVSn/NiTiSn	1.05	Co TiSn	17	0.00	0.00	0.00	-0.5	HG	VSn Ni	19	-0.01	0.58	0.53	0.5	SPEG

constants by Ma *et al.* in Ref. [19] (their values were 0.38, 0.44, 0.65, and 1.06 respectively). This shows that the adopted electronic band structure method for the calculations is not crucial to calculate the properties and results depend strongly on the choice of the exchange-correlation functional; in both studies (ours and the study of Ma *et al.*) the PBE parametrization of the GGA functional has been used). Moreover, our result for CoTiSb agrees well with the experimental value of about 1 eV [30]. Finally, in Table I, we have also included the relative position of the VBM and CBM with respect to the Fermi level calculated as the Fermi level minus the corresponding energy VBM position and this explains why the E_{VB} has a negative sign while E_{CB} has a positive sign.

B. Spin-polarized 2DEG and 2DHG at the Interfaces

The study of the bulk systems is followed by the calculation of the interface properties of heterojunctions. First, in Fig. 3, we present the band alignment of all considered heterojunctions. Our four compounds result in six possible heterojunctions and among them only FeVSb/CoTiSb and CoTiSb/NiTiSn possess type-I band alignment meaning that the CBM of FeVSb (NiTiSn) is higher than the CBM of CoTiSb, and the VBM of both FeVSb and NiTiSn is lower in energy than the VBM of CoTiSb. All other four heterojunctions are of Type-II character. Note that the band alignment of the heterojunctions is calculated according to the procedure presented in Ref. [44]. We have simulated the interfaces as discussed in detail in Section II and in Table II we summarize all our results. First, we should note that for each heterostructure, there are two possible terminations at the interface denoted as Termination-1 when the first compound ends at a pure X layer and Termination-2 when it ends at a mixed YZ layer. As we discussed above in Section II the second compound adopts the in-plane lattice constant of the first compound, and its out-of-plane lattice constant changes accordingly in order to preserve the unit cell volume as shown by the c/a ratios presented in Table II.

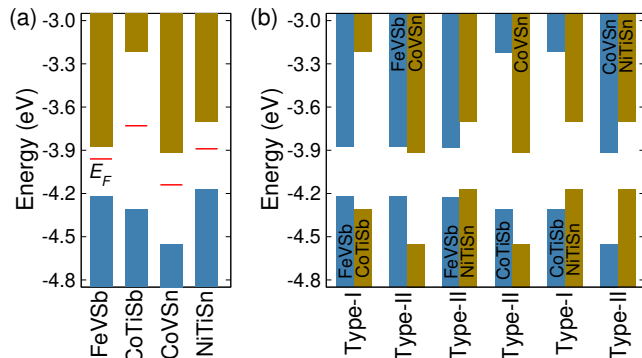


FIG. 3. (a) Position of the valence and conduction bands with respect to the Fermi level in bulk Heusler compounds. (b) Band alignment for the various interfaces under study. Type-I and type-II denote the two possible types of band alignment (see text for details).

With the exception of the CoTiSb/CoVSn case, in all other studied heterojunctions, the number of valence electrons at the interface is no more 18 but there is either an excess of electrons (Z_t taking into account the two layers which form the interface is larger than 18) or a deficit of electrons (Z_t is smaller than 18) and the interface is metallic. In the first case of electron excess, we should have the creation of a 2DEG, while electron deficit can be translated to an excess of holes leading to 2DHG. But as the band structures projected on the (001) plane and presented in Fig. 4 reveal the situation is more complex. In most cases, the metallic interface is also magnetic and the 2DEG (2DHG) is spin-polarized.

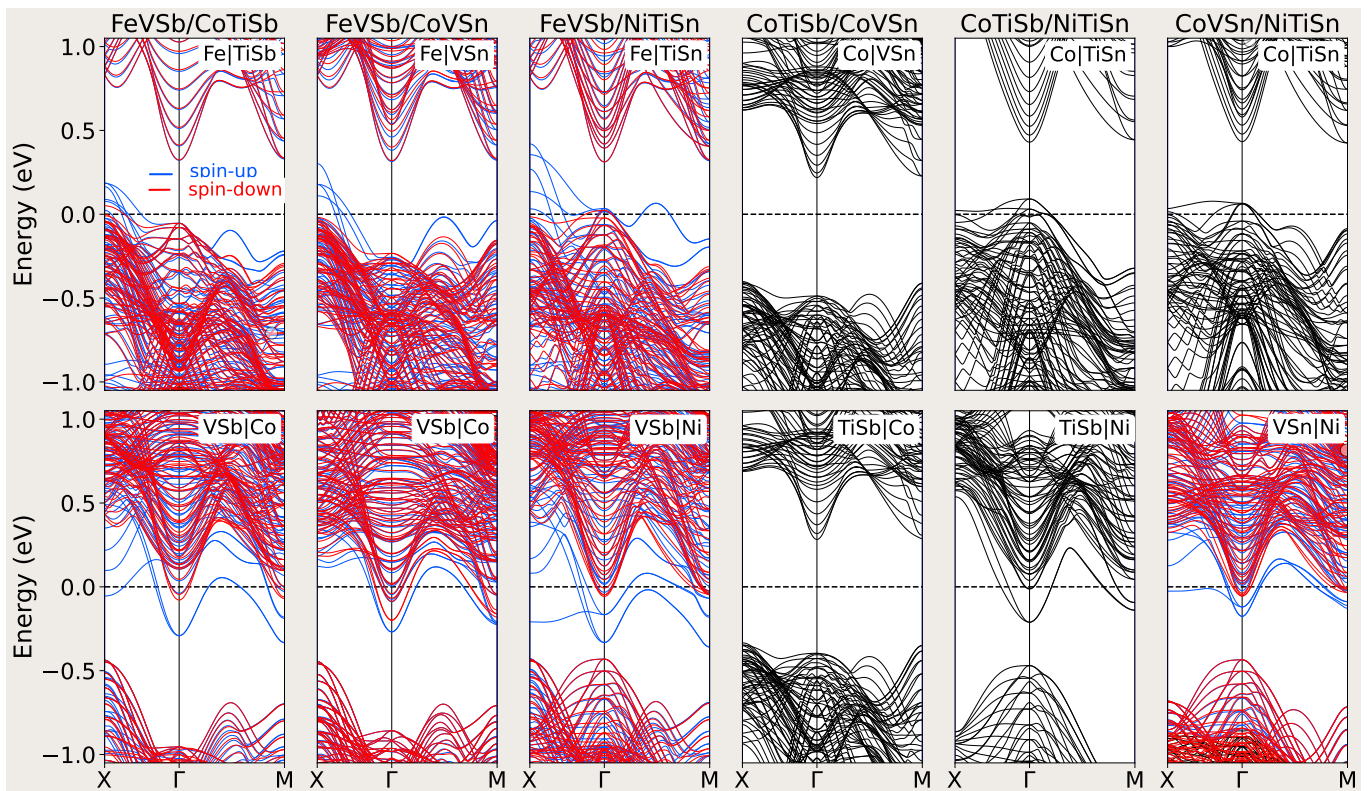


FIG. 4. Band structure for all considered heterojunctions along the X- Γ -M high symmetry directions of the 2D Brillouin zone.

In Table II we present also the spin magnetic moments of the atoms at the two interface layers as well as the total spin magnetic moment taking the sum of the spin moments of all interface atoms.

The heterojunctions where FeVSb is one of the two junction materials are the most interesting cases. When Fe is at the interface, there is a deficit of electrons and we have a 2D spin-polarized hole gas (SPHG). In the band structures shown in Fig. 4 this is reflected in the conduction bands, which are crossed by the Fermi level. When the interface layer is VSb and not Fe, there is an excess of electrons leading to 2D spin-polarized electrons gas (SPEG) and now the Fermi level crosses the valence bands. Moreover, the Fe and V atoms of FeVSb at the interface and subinterface layers are the ones responsible for the spin-polarized character of the electron (hole) gas. This is depicted clearly in Fig. 5, where we present a schematic representation of the layers around the interface for all three heterojunctions containing FeVSb and for both terminations. Arrows show the direction of the atomic spin magnetic moments and their magnitude is proportional to the values of the spin magnetic moments. In all three heterojunctions presented in the figure, it is easily observed that the magnetic moments reside primarily at the Fe and V atoms at the interface and subinterface layers irrespective of whether we have Fe (Termination-1) or VSb (Termination-2) interface layers.

In the case of Termination-I interfaces, the Fe atoms

at the interface layer carry sizeable magnetic moments which are antiparallel to the spin magnetic moments

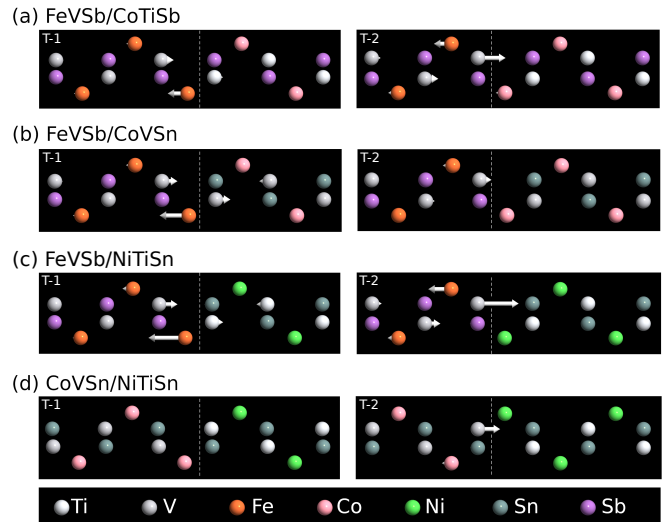


FIG. 5. (Color online) For both possible interface structures (denoted as T1 and T2) for each system, we show the structure of the interfaces. Arrows denote the direction of the spin magnetic moments of the atoms at the interface and their magnitude is proportional to the absolute value of the atomic spin magnetic moments presented in Table II.

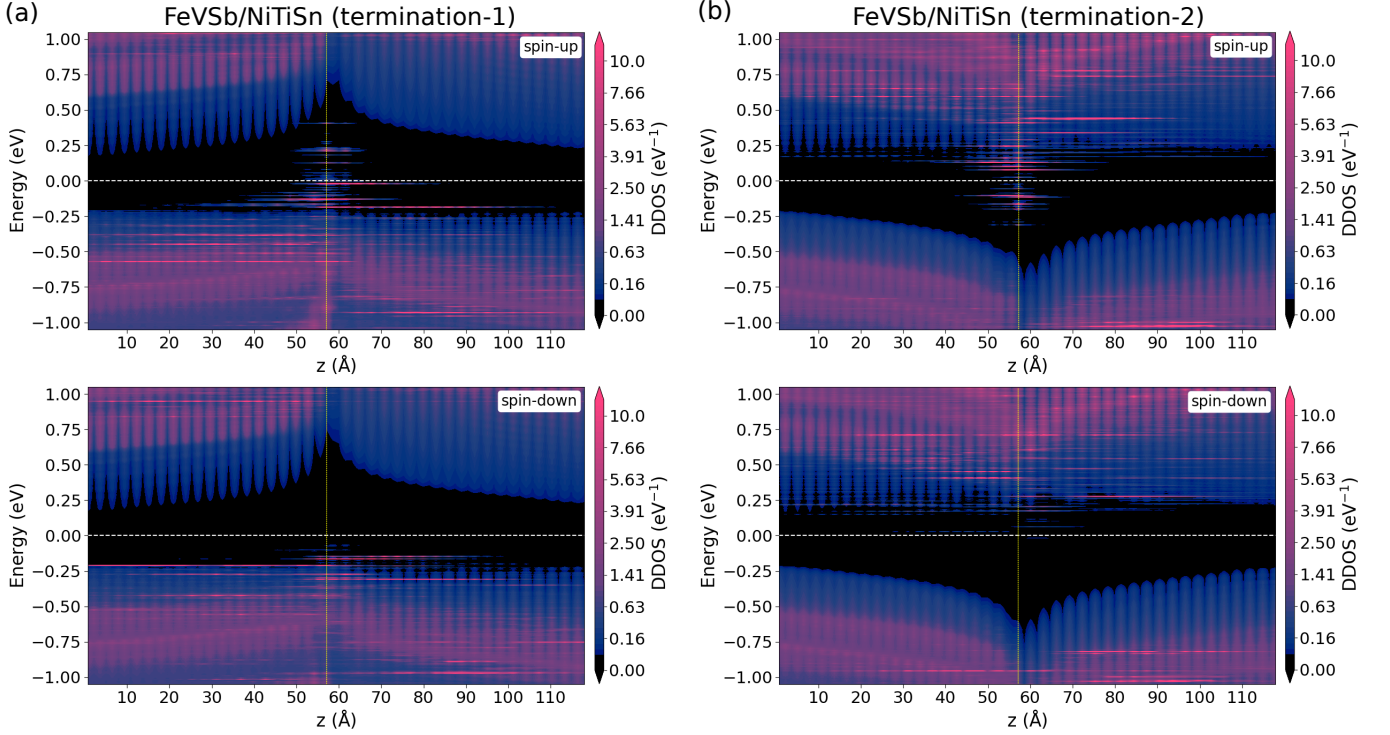


FIG. 6. (a) (Color online) Projected device density of states (DDOS) for the spin-up (upper panel) and spin-down electrons (lower panel) for the first termination of the FeVSb/NiTiSn junction (the atomic structure for the interface region is given in 5). The white dashed lines display the Fermi level while the vertical yellow dashed lines denote the interface. (b) The same as (a) for the second termination.

of the Ti (V) interface atoms as shown in Table II and schematically in Fig. 5. In the case of Termination-2 interfaces the Co (Ni) atoms carry very small spin magnetic moments and it is the V atom at the interface layer of FeVSb, which carries again the main portion of the spin magnetic moment. CoVSb/CoTiSb is a particular case due to the presence of Co in both materials of the heterojunction, and the resulting interface remains semiconducting for both terminations (see Fig. 4). In the case of CoTiSb/NiTiSn interfaces the interface is metallic but non-spin-polarized and thus we have either a usual 2DEG or 2DHG behavior at the interface as shown in Table II and as can be deduced from Fig. 4. Finally, in the case of the CoVSb/NiTiSn, termination-II is spin-polarized and the 2DEG is also spin-polarized, while termination-I is simply metallic, as deduced also from the band structure in Fig. 4, and there is a usual 2DHG at the interface.

To confirm our conclusions we have also performed device calculations for both possible terminations in the case of the FeVSb/NiTiSn heterostructure. As discussed in Section II device calculations are much more demanding in computer resources than the supercell calculations presented up to now. In this case, we have a 120 Å heterojunction (i.e., the scattering region) with two semi-infinite leads. The obtained spin magnetic moments are similar to the ones obtained using the supercell approach shown in Table II. In Fig. 6 we present for both termi-

nations the spin-up and the spin-down device density of states (DDOS) as a function of the distance. For the spin-up DOS (upper panels) there is a finite DOS around the interface layers which quickly vanishes as we move away from the interface. In the case of the spin-down DOS for both terminations (lower panels) there is a negligible DOS around the Fermi level around the interface region of the device. Thus at the interface, we have a nearly half-metallic magnetic behavior and as we move away from the interface we get non-magnetic semiconducting behavior.

The results discussed in the previous paragraph agree well with the conclusions in Ref. [44] regarding the confinement of the electrons and holes at the interface. In Ref. [44] the authors have studied the case of CoTiSb/NiTiSn heterojunction. At the TiSb-Ni interfaces, which accommodates a 2DEG, electrons are confined in a region of about 1.5 nm (15 Å) around the interface layer. At the Co-TiSn interface, there is a 2DHG and the holes are confined in a slightly larger region of about 20 Å around the interface. In our case of FeVSb/NiTiSn heterojunction, as shown in Fig. 6, the change in the DDOS around the interface layer occurs in a region of about 20 Å around the Fermi level in the case of the Fe-TiSn interface and a slightly thicker region in the case of the VSb-Ni interface. Thus the electron and hole gas are confined in a similar region as in Ref. [44].

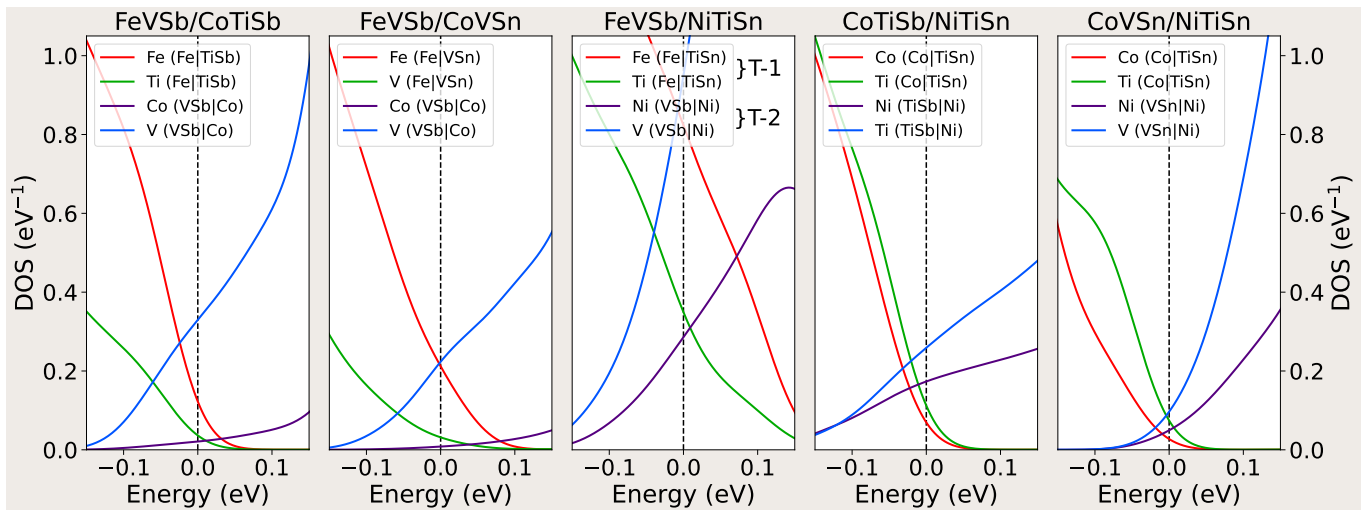


FIG. 7. Atom-resolved non-magnetic (paramagnetic) total density of states (DOS) of the transition metal atoms at the two interface layers around the Fermi level of the heterojunctions.

C. Origin of the spin-polarization at the interface

The emergence of interface spin polarization can be qualitatively explained on the basis of the Stoner model for itinerant ferromagnetism. In materials where the Stoner criterion is fulfilled ($I \cdot N(E_F) > 1$, where I is the Stoner parameter and $N(E_F)$ is the non-spin-polarized DOS at the Fermi level), the occurrence of magnetism is favored. To examine whether the Stoner model can be applied to the interfaces one should first estimate the value of I and $N(E_F)$. For the latter in Fig. 7 we have plotted the non-spin-polarized DOS around the Fermi level for the atoms at the interface of heterojunctions except the CoTiSb/CoVSn one which is a non-magnetic semiconductor. One can easily see that the FeVSb/NiTiSn heterojunction for both terminations presents a significantly larger DOS at the Fermi level than all other cases which approach the value of 1 eV^{-1} .

To estimate the value of the Stoner parameter I , we can use the relationship $I = \frac{U+6J}{5}$ proposed by Stollhoff *et al.*, where U is and J are the Hubbard on-site Coulomb repulsion and the exchange parameters, respectively. These parameters are hard to extract experimentally and their *ab-initio* calculation is very demanding. In Ref. [69], their values have been calculated for several Heusler materials including also some half-Heusler compounds using the constrained random-phase-approximation. For the transition metal atoms of half-Heusler compounds the U parameters calculated in Ref. [69] vary between 3 eV and 4 eV and the J parameter is around 0.7 eV. We expect that since these values are for bulk systems, in the case of 2D systems like the ones studied here, the U values will be slightly larger due to reduced screening stemming from the out-of-plane atoms in the heterojunctions. Thus, using the U and J values from the Ref. [69] the relation mentioned above gives for the I parameter a value of 1 eV to 1.4 eV. According to

this, we should expect that only the two terminations of the FeVSb/NiTiSn heterojunction should present a spin-polarized electronic band structure at the interface. But the Stoner model for itinerant magnetism is a mean-field treatment missing the effect of strong electronic correlations. The latter can induce also magnetic order [70] as it seems to be the case for all the other interfaces which present a low DOS at the Fermi level as shown in Fig. 6 and do not fulfill the Stoner criterion.

D. Modified Slater-Pauling Rules for Interfaces

Slater-Pauling rules in the case of Heusler compounds were initially formulated in the case of half-metallic Heuslers crystallizing in the $C1_b$ lattice as the one adopted by the present compounds [13]. These rules connect the half-metallicity and the magnetic properties in the case of Heusler compounds. It was shown in Ref. [13] that the total spin magnetic moment in the unit cell M_t in μ_B units is just the total number of valence electrons in the unit cell, Z_t minus 18 for half-metals ($M_t = Z_t - 18$). This rule expresses the fact that in the spin-down band structure, where the energy gap exists, there are exactly 9 completely occupied bands. When Z_t equals 18 the total spin magnetic moment is zero. Since in the Heusler compounds crystallizing in the $C1_b$ lattice, conventional antiferromagnetism cannot occur due to symmetry reasons, the 18 valence electron Heusler compounds have to be semiconductors or completely compensated ferrimagnetic half metals. This prediction is in agreement with the behavior of FeVSb, CoVSn, CoTiSb, and NiTiSn compounds.

The question which rises is whether it is possible to formulate the Slater-Pauling rule in a way to connect the magnetic properties of the studied heterojunctions with the total number of valence electrons at the inter-

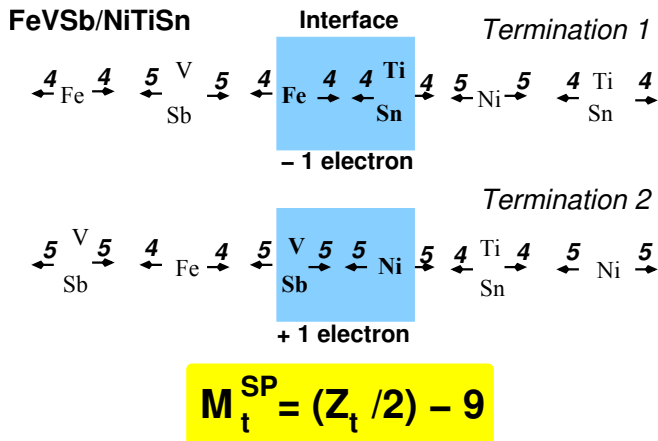


FIG. 8. Schematic representation of the bonding in the two possible FeVSb-NiTiSn interfaces. For the half-metallic materials from both sites of the interface the bonds between the atoms at two consecutive layers are built up from 9 valence electrons. The numbers on top of the arrows show the valence electrons contributed by each layer (e.g. VSb has ten valence electrons which are splitted for the bonds at the two sides of the VSb layer). At the interface, the electrons contributing at the bonding are $\frac{Z_t}{2}$ (see Table II for the definition). Thus the excess or shortage of valence electrons at the interface with respect to the nine within the rest of the material is $\frac{Z_t}{2} - 9$. To achieve half metallicity these extra(less) valence electrons should occupy(vacate) spin-up states leading to a modified Slater-Pauling rule for the total spin magnetic moment at the interface: $M_t^{\text{SP}} = \frac{Z_t}{2} - 9$ where M_t^{SP} is in μ_B .

face. To answer this question, one should consider the (001) planes of the lattice shown in Fig. 1 and we will use FeVSb as the example. The (001) planes are made up either of pure Fe or mixed V-Sb atoms. The FeVSb unit cell has in total 18 valence electrons; Fe contributes 8 valence electrons and the V-Sb atoms 10. In a simplified representation like the one shown in Fig. 8, each Fe plane contributes 4 electrons to the bonds with the VSb plane on its right and another 4 electrons to build up bonds with the VSb plane on its left. Following the same reasoning, each VSb plane contributes 5 electrons to each one of its two sides. Thus in total 9 electrons contribute to the bonding between the atoms in two consecutive layers. The same reasoning stands also for NiTiSn but now Ni planes contribute 5 electrons to the bonds with each one of the neighboring TiSn layers and each TiSn layer contributes 4 electrons to the corresponding bonds. At the VSb-Ni or TiSn-Fe interfaces shown in Fig. 7 we have now 10 or 8 electrons, respectively, contributing to the bonding between the atoms at the interface layers. The total number of these electrons is $Z_t/2$, where Z_t refers to the compound built up from the atoms at the interface (e.g. NiVSb or FeTiSn in our case) and thus the difference with the nine electrons of the perfect semiconducting interface is $Z_t/2 - 9$. This means that at the VSb-Ni interface, there is a surplus of one electron, while at the TiSn-Fe interface, there is a shortage

of one electron. Thus the prerequisite for half-metallicity at the interfaces is that the total spin magnetic moment at the interface follows a modified Slater-Pauling rule of the $M_t = Z_t/2 - 9$ form.

To verify the validity of the proposed modified Slater-Pauling rule in Table II we present the calculated total spin magnetic moment for all interfaces with respect to the ones predicted by the Slater-Pauling rule. For the discussion, we take into account the electronic character of the interface as presented in Fig. 4 where the (001) projected band structures for all interfaces are presented. The calculated total spin magnetic moments are very close to the ones predicted by the Slater-Pauling rule for half-metallic behavior (deviation less than $0.05 \mu_B$) in the case where FeVSb is part of the heterojunction and Fe is at the interface as well as for the VSb-Ni interface. If we examine the band structures presented in Fig. 4 the Fe-VSn interface is a perfect half-metal. In the case of Fe-TiSb interface, the Fermi level slightly crosses the spin-down conduction band, while in the case of VSb-Co and VSb-Ni interfaces, the Fermi level slightly crosses the spin-down conduction band. Both types of interfaces between the CoTiSb and CoVSb compounds are semiconducting in agreement with the Slater-Pauling rule. For the rest of the interfaces, the Slater-Pauling rule is not obeyed and the electronic character of the interfaces is no more half-metallic. Magnetism in materials appears when the gain in energy due to the lowering of the DOS at the Fermi level (fewer electrons with the maximum energy) overcomes the cost in band energy (energy to flip spins and create the spin imbalance needed for magnetism). In half-metallic magnets, the magnitude of both competing energy contributions increases but the final gain in energy is larger than in the simple magnetic case. Otherwise, the material remains magnetic without being half-metallic explaining the different behavior of the interfaces under study.

E. Exchange Interactions and Curie Temperature

In the last part of our study, we compute the Heisenberg exchange parameters as discussed in detail in Section II. We have chosen the FeVSb/CoTiSb and FeVSb/NiTiSn heterojunctions since both follow the modified Slater-Pauling rule described above. We present our results in Fig. 9. The upper panels refer to Termination-1, where the interface is Fe-TiSb (TiSn) and the lower panels to Termination-2, where the interface layers are VSb-Co(Ni). We restrict ourselves to FeVSb only, since only the Fe and V atom at the interface present significant spin magnetic moments, and present the exchange constants as a function of the distance for the Fe and V atoms at the interface and sub-interface layers. The first striking characteristic feature in all cases is the strong negative exchange parameters between the nearest neighbor Fe-V atoms. This is reflected in the antiparallel Fe-V spin magnetic moments

TABLE III. Calculated magnetic anisotropy energy (MAE) and the interface Curie temperature T_C for the FeVSb/CoTiSb (NiTiSn) heterojunctions for both possible interface terminations.

Half-Heusler heterojunction	Interface termination	MAE=($E_{ }$ - E_{\perp}) (μ eV/cell)	T_C (K)
FeVSb/CoTiSb	Fe TiSb	-121.3	78
	VSb Co	-76.6	101
FeVSb/NiTiSn	Fe TiSn	8.5	187
	VSb Ni	-24.9	248

which stabilize the magnetic order at the interface. In the case of Termination-1, the V atoms are at the subinterface layer, the V has negligible spin magnetic moments and the V-V exchange constants are vanishing. In the case of Termination-2, the V atoms are at the interface layer and they carry a sizeable spin magnetic moment as shown in Table II (see also Fig. 5) and the V-V exchange interactions are all positive, favoring the ferromagnetic alignment of the V spin magnetic moments. For Termination-2, the interactions between the Fe atoms located at the subinterface layer are negligible as expected. Interestingly in the Termination-1 cases, the Fe-Fe exchange parameters are sizeable for both FeVSb/CoTiSb and FeVSb/NiTiSn heterojunctions favoring the ferromagnetic alignment of the Fe spin magnetic moments at the interface layers.

We used the calculated exchange parameters to esti-

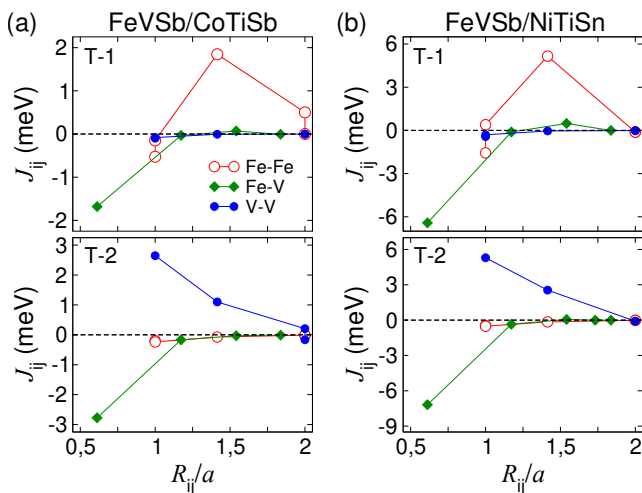


FIG. 9. (a) (Color online) Calculated intra-sublattice (Fe-Fe and V-V) and inter-sublattice (Fe-V) Heisenberg exchange parameters as a function of distance for the interface and subinterface layers of the FeVSb/CoTiSb heterojunction for both possible T-1 and T-2 interface terminations. (b) The same as (a) for the FeVSb/NiTiSn heterojunction. For the definition of T-1 and T-2 see Figs. 1 and 5.

mate the Curie temperature T_C within the mean-field approximation (MFA) and present our results in Table III. The obtained values range from about 78 K to about 248 K being larger for the FeVSb/NiTiSn heterostructure and for Termination-2 with respect to Termination-1. These values are relatively small when compared to room temperature. Unfortunately, no experimental data on the Curie temperatures exist in the literature for comparison to establish the accuracy of our calculations. Such a comparison would be necessary since (i) MFA ignores spin-fluctuations which are important especially for low-dimensional magnets tending to overestimate T_C , and (ii) for systems with small spin magnetic moments (less than $1 \mu_B$), the exchange parameters J_{ij} are underestimated when using the linear response theory (as is the case here) and thus the T_C is also underestimated [71]. These two phenomena induce competing errors and this explains the behavior of calculated T_C in bulk half-ferromagnetic Heusler compounds; in the case of NiMnSn where the Mn spin magnetic moment is very large the MFA overestimates the T_C by about 400 K, while in Co_2CrAl and Co_2MnSi full-Heusler compounds due to the much smaller spin magnetic moments, MFA is much more accurate and underestimates T_C by about 50-100 K only [72]. In the case of the studied interfaces due to the small spin magnetic moments at the interface, we expect that the errors induced by the two competing phenomena will almost cancel out each other and the agreement with the experiment will be even better than in full-Heusler compounds.

Finally, in Table. III we also present the calculated values of the magnetic anisotropy energy (MAE) for FeVSb in μ eV per cell. All systems possess small values of MAE of the order of $0.1 m$ eV. In all cases, the easy magnetization axis is perpendicular to the interface with the exception of Termination-1 in the FeVSb/NiTiSn system where the easy magnetization axis is parallel to the interface but the MAE is almost vanishing. As discussed above when we considered our supercells, FeVSb adopted in all studied cases a cubic lattice and we relaxed the cell only of the other material in the heterojunction. This explains the very small calculated MAE values. If the vice-versa procedure takes place and now FeVSb is grown on top of the other material (*e.g.* CoTiSb), the latter will adopt a cubic lattice and FeVSb will adopt the same in-plane lattice constant. This will lead to a tetragonal structure for the FeVSb material and much larger MAE values [12], since materials tend to keep their unit cell volume almost constant and change accordingly their lattice parameters.

IV. SUMMARY AND CONCLUSIONS

Half-Heusler compounds, which have 18 valence electrons per unit cell, like FeVSb, CoTiSb, CoVSb and NiTiSn are well-known for their non-magnetic semiconducting properties. In the present study, we employed first-principles electronic band structure calculations and ex-

amined the properties of the interfaces of the heterojunctions based on these four half-Heusler compounds. First, we confirmed the non-magnetic semiconducting character of these compounds in their bulk form. Then we used a supercell approach to study the heterojunction interfaces considering the [001] axis as the growth direction. Our results showed that several of these interfaces become metallic and in several cases also magnetic. The emergence of spin polarization is accompanied by the formation of a two-dimensional electron (2DEG) or hole (2DHG) gas at the interface making such structures promising for spintronic applications.

To further understand the magnetic properties of the interfaces of heterojunctions, we developed a modified Slater-Pauling rule that is similar to the corresponding rule for the bulk half-metallic half-Heusler compounds. This rule connects the altered number of valence electrons at the interface to the total spin magnetic moment at the interface and is a prerequisite for half-metallicity to occur. We also calculated other properties of interest, such as exchange parameters, Curie temperature, and magnetic anisotropy energies.

Overall, our study adds to the growing body of knowledge on the properties of half-Heusler heterojunction interfaces and their potential for use in spintronic and mag-

netoelectronic devices. We hope that our findings, combined with recent experimental evidence for the presence of 2DEG at CoTiSb/NiTiSn heterojunctions [50], will increase interest in these materials and their potential applications. We expect our study to motivate future efforts and studies toward the experimental realization of devices using the proposed heterojunctions.

ACKNOWLEDGMENTS

This work was supported by SFB CRC/TRR 227 of Deutsche Forschungsgemeinschaft (DFG) and by the European Union (EFRE) via Grant No: ZS/2016/06/79307. B. S. acknowledges financial support from Swedish Research Council (grant no. 2022-04309). The computations were enabled in project SNIC 2021/3-38 by resources provided by the Swedish National Infrastructure for Computing (SNIC) at NSC, PDC, and HPC2N partially funded by the Swedish Research Council (Grant No. 2018-05973). B.S. acknowledges allocation of supercomputing hours by PRACE DECI-17 project ‘Q2Dtopomat’ in Eagle supercomputer in Poland and EuroHPC resources in Karolina supercomputer in Czech Republic.

-
- [1] F. Heusler, Kristallstruktur und Ferromagnetismus der Mangan-Aluminium-Kupferlegierungen, *Verh. Dtsch. Phys. Ges.* **12**, 219 (1903).
- [2] F. Heusler and E. Take, The nature of the Heusler alloys, *Phys. Z.* **13**, 897 (1912).
- [3] T. Graf, C. Felser, and S. S. P. Parkin, Simple rules for the understanding of Heusler compounds, *Progr. Sol. St. Chem.* **39**, 1 (2011).
- [4] S. Tavares, K. Yang, and M. A. Meyers, Heusler alloys: Past, properties, new alloys, and prospects, *Progr. Mat. Sci.* **132**, 101017 (2023).
- [5] S. Chatterjee, S. Chatterjee, S. Giri, and S. Majumdar, Transport properties of Heusler compounds and alloys, *J. Phys.: Condens. Matter* **34**, 013001 (2022).
- [6] M. Katsnelson, V. Y. Irkhin, L. Chioncel, A. Lichtenstein, and R. A. de Groot, Half-metallic ferromagnets: From band structure to many-body effects, *Rev. Mod. Phys.* **80**, 315 (2008).
- [7] I. Galanakis, K. Özdoğan, and E. Şaşıoğlu, Spin-filter and spin-gapless semiconductors: The case of Heusler compounds, *AIP Advances* **6**, 055606 (2016).
- [8] E. Şaşıoğlu, S. Blügel, and I. Mertig, Proposal for reconfigurable magnetic tunnel diode and transistor, *Appl. Electron. Mater.* **1**, 1552 (2019).
- [9] E. Şaşıoğlu, T. Aull, D. Kutschabsky, S. Blügel, and I. Mertig, Half-Metal–Spin-Gapless-Semiconductor Junctions as a Route to the Ideal Diode, *Phys. Rev. Appl.* **14**, 014082 (2020).
- [10] J. K. Kawasaki, Heusler interfaces—Opportunities beyond spintronics?, *APL Mater.* **7**, 080907 (2019).
- [11] T. Aull, E. Şaşıoğlu, I. Maznichenko, S. Ostanin, A. Ernst, M. I. and G. I, Ab initio design of quaternary Heusler compounds for reconfigurable magnetic tunnel diodes and transistors, *Phys. Rev. Materials* **3**, 124415 (2019).
- [12] T. Aull, E. Şaşıoğlu, and I. Mertig, First principles design of Ohmic spin diodes based on quaternary Heusler compounds, *Appl. Phys. Lett.* **118**, 052405 (2021).
- [13] I. Galanakis, P. Dederichs, and N. Papanikolaou, Origin and properties of the gap in the half-ferromagnetic Heusler alloys, *Phys. Rev. B* **66**, 134428 (2002).
- [14] I. Galanakis, P. Dederichs, and N. Papanikolaou, Slater-Pauling behavior and origin of the half-metallicity of the full-Heusler alloys, *Phys. Rev. B* **66**, 174429 (2002).
- [15] I. Galanakis, Appearance of half-metallicity in the quaternary Heusler alloys, *J. Phys.: Condens. Matter* **16**, 3089 (2004).
- [16] S. Skaftouros, K. Ozdogan, E. Şaşıoğlu, and I. Galanakis, Generalized Slater-Pauling rule for the inverse Heusler compounds, *Phys. Rev. B* **87**, 024420 (2013).
- [17] K. Ozdogan, E. Şaşıoğlu, and I. Galanakis, Slater-Pauling behavior in LiMgPdSn-type multifunctional quaternary Heusler materials: Half-metallicity, spin-gapless and magnetic semiconductors, *J. Appl. Phys.* **113**, 193903 (2013).
- [18] S. Nepal, R. Dhakal, I. Galanakis, S. M. Winter, R. P. Adhikari, and G. C. Kaphle, Ab initio study of stable 3d, 4d, and 5d transition-metal-based quaternary Heusler compounds, *Phys. Rev. Materials* **6**, 114407 (2022).
- [19] J. Ma, V. I. Hegde, K. Munira, Y. Xie, S. Keshavarz, D. T. Mildebrath, C. Wolverton, A. W. Ghosh, and W. H. Butler, Computational investigation of half-Heusler compounds for spintronics applications, *Phys. Rev. B* **95**, 024411 (2017).

- [20] M. Gilleßen and R. Dronskowski, A combinatorial study of full Heusler alloys by first-principles computational methods, *J. Comput. Chem.* **30**, 1290 (2009).
- [21] M. Gilleßen and R. Dronskowski, A combinatorial study of inverse Heusler alloys by first-principles computational methods, *J. Comput. Chem.* **31**, 612 (2010).
- [22] S. V. Faleev, Y. Ferrante, J. Jeong, M. G. Samant, B. Jones, and S. S. P. Parkin, Unified explanation of chemical ordering, the Slater-Pauling rule, and half-metallicity in full Heusler compounds, *Phys. Rev. B* **95**, 045140 (2017).
- [23] S. V. Faleev, Y. Ferrante, J. Jeong, M. G. Samant, B. Jones, and S. S. P. Parkin, Origin of the tetragonal ground state of Heusler compounds, *Phys. Rev. Appl.* **7**, 034022 (2017).
- [24] S. V. Faleev, Y. Ferrante, J. Jeong, M. G. Samant, B. Jones, and S. S. P. Parkin, Heusler compounds with perpendicular magnetic anisotropy and large tunneling magnetoresistance, *Phys. Rev. Mater.* **1**, 024402 (2017).
- [25] Q. Gao, I. Opahle, and H. Zhang, High-throughput screening for spin-gapless semiconductors in quaternary Heusler compounds, *Phys. Rev. Mater.* **3**, 024410 (2019).
- [26] Y. Han, Z. Chen, M. Kuang, Z. Liu, W. X., and X. Wang, 171 Scandium-based full Heusler compounds: A comprehensive study of competition between XA and L₂₁ atomic ordering, *Res. in Phys.* **12**, 435 (2019).
- [27] D. Jung, H.-J. Koo, and M.-H. Whangbo, Study of the 18-electron band gap and ferromagnetism in semi-Heusler compounds by non-spin-polarized electronic band structure calculations, *J. Mol. Struct.:THEOCHEM* **527**, 113 (2000).
- [28] J. Pierre, R. V. Skolozdra, Y. K. Gorelenko, and M. Kouacou, From nonmagnetic semiconductor to itinerant ferromagnet in the TiNiSn-TiCoSn series, *J. Magn. Mater.* **134**, 95 (1994).
- [29] J. Tobola, J. Pierre, S. Kaprzyk, R. Skolozdra, and M. Kouacou, Crossover from semiconductor to magnetic metal in semi-Heusler phases as a function of valence electron concentration, *J. Phys.: Condens. Matter* **10**, 1013 (1998).
- [30] S. Ouardi, G. H. Fecher, C. Felser, M. Schwall, S. S. Naghavi, A. Gloskovskii, B. Balke, J. Hamrle, K. Postava, J. Pištora, S. Ueda, and K. Kobayashi, Electronic structure and optical, mechanical, and transport properties of the pure, electron-doped, and hole-doped Heusler compound CoTiSb, *Phys. Rev. B* **86**, 045116 (2012).
- [31] C. Lue, Y. Oner, D. Naugle, and J. Ross, Magnetism of new semi-Heusler compounds FeVSn and CoVSn, *IEEE Trans. Magn.* **37**, 2138 (2001).
- [32] M. Mokhtari, F. Dahmane, G. Benabdellah, L. Zekri, S. Benalia, and N. Zekri, Theoretical study of the structural stability, electronic and magnetic properties of XVsb ((X = Fe, Co, and Ni) half-Heusler compounds, *Condens. Matter Phys.* **11**, 43705 (2018).
- [33] E. H. Shourov, R. Jacobs, W. A. Behn, Z. J. Krebs, C. Zhang, P. J. Strohbeen, D. Du, P. M. Voyles, V. W. Brar, D. D. Morgan, and J. K. Kawasaki, Semiadsorption-controlled growth window for half-Heusler FeVSb epitaxial films, *Phys. Rev. Materials* **4**, 073401 (2020).
- [34] K. Kroth, B. Balke, G. H. Fecher, V. Ksenofontov, C. Felser, and H.-J. Lin, Diluted magnetic semiconductors with high curie temperature based on C1(b) compounds: CoTi_{1-x}Fe_xSb, *Appl. Phys. Lett.* **89**, 202509 (2006).
- [35] N. Naghibolashrafi, V. I. Hegde, K. C. Shambhu, S. Keshavarz, S. S. Naghavi, J. Ma, A. Gupta, P. LeClair, W. H. Butler, C. Wolverton, K. Munira, D. Mazumdar, and A. W. Ghosh, Structural and magnetic analyses of the Fe_xCo_{1-x}TiSb alloy system: Fe_{0.5}Co_{0.5}TiSb as a prototypical half-Heusler compound, *J. All. Comp.* **822**, 153408 (2020).
- [36] B. Nanda and I. Dasgupta, Electronic structure and magnetism in doped semiconducting half-Heusler compounds, *J. Phys.: Condens. Matter* **17**, 5037 (2005).
- [37] B. Sanyal, O. Eriksson, K. G. Suresh, I. Dasgupta, A. K. Nigam, and P. Nordblad, Ferromagnetism in Mn doped half-Heusler NiTiSn: Theory and experiment, *Appl. Phys. Lett.* **89**, 212502 (2006).
- [38] N. Y. Sun, Y. Q. Zhang, W. R. Che, J. Qin, and R. Shan, Structural, magnetic, and transport properties of Fe-doped CoTiSb epitaxial thin films, *J. Appl. Phys.* **118**, 173905 (2015).
- [39] N. Tareuchi, K. Goshō, M. Hiroi, and M. Kawakami, The effect of V substitution on the properties of CoTiSb, *Phys. Rev. B* **359**, 1183 (2005).
- [40] J. Tobola and J. Pierre, Electronic phase diagram of the XTZ (X=Fe, Co, Ni; T=Ti, V, Zr, Nb, Mn; Z=Sn, Sb) semi-Heusler compounds, *J. All. Comp.* **296**, 243 (2000).
- [41] J. Tobola, S. Kaprzyk, and P. Pecheur, Theoretical search for magnetic half-Heusler semiconductors, *Phys. St. Sol. B* **236**, 531 (2003).
- [42] B. Balke, G. H. Fecher, A. Gloskovskii, J. Barth, K. Kroth, C. Felser, R. Robert, and A. Weidenkaff, Doped semiconductors as half-metallic materials: Experiments and first-principles calculations of CoTi_{1-x}M_xSb (M = Sc, V, Cr, Mn, Fe), *Phys. Rev. B* **77**, 045209 (2008).
- [43] Z. Zhu, Y. Cheng, and U. Schwingenschloegl, Vacancy induced half-metallicity in half-Heusler semiconductors, *Phys. Rev. B* **84**, 113201 (2011).
- [44] A. Sharan, Z. Gui, and A. Janotti, Formation of two-dimensional electron and hole gases at the interface of half-Heusler semiconductors, *Phys. Rev. B Materials* **3**, 061602 (2019).
- [45] J. Betancourt, T. R. Paudel, E. Tsybal, and J. P. Velev, Spin-polarized two-dimensional electron gas at GdTlO₃/SrTiO₃ interfaces: Insight from first-principles calculations, *Phys. Rev. B* **96**, 045113 (2017).
- [46] A. Ohtomo, D. A. Muller, J. L. Grazul, and H. Hwang, Artificial charge-modulation in atomic-scale perovskite titanate superlattices, *Nature* **419**, 378 (2002).
- [47] A. Ohtomo and H. Hwang, A high-mobility electron gas at the LaAlO₃/SrTiO₃ heterointerface, *Nature* **427**, 423 (2004).
- [48] N. T. Linh, The two-dimensional electron gas and its technical applications, in *Festkörperprobleme 23: Plenary Lectures of the Divisions "Semiconductor Physics" "Metal Physics" "Low Temperature Physics" "Thermodynamics and Statistical Physics" "Thin Films" "Surface Physics" "Surface Physics" "Magnetism" of the German Physical Society (DPG) Freudenstadt, March 21.-25., 1983*, edited by P. Grosse (Springer Berlin Heidelberg, 1983) pp. 227–257.
- [49] S. Keshavarz, I. Di Marco, D. Thonig, L. Chioncel, O. Eriksson, and Y. O. Kvashnin, Magnetic two-dimensional electron liquid at the surface of Heusler semiconductors, *Phys. Rev. Materials* **4**, 021401 (2020).

- [50] S. D. Harrington, *Semiconducting Half-Heusler Based Compounds and Heterostructures Grown by Molecular Beam Epitaxy*, Ph.D. thesis, University of California Santa Barbara (2018).
- [51] S. Jenkins, L. Rozsa, U. Atxitia, R. F. L. Evans, K. S. Novoselov, and E. J. G. Santos, Breaking through the Mermin-Wagner limit in 2D van der Waals magnets, *Nature Commun.* **13**, 6917 (2022).
- [52] G. Kresse and J. Hafner, Norm-Conserving and Ultrasoft Pseudopotentials for First-Row and Transition Elements, *J. Phys.: Condens. Matter* **6**, 8245 (1994).
- [53] G. Kresse and D. Joubert, From Ultrasoft Pseudopotentials to the Projector Augmented-Wave Method., *Phys. Rev. B* **59**, 1758 (1999).
- [54] J. P. Perdew, K. Burke, and M. Ernzerhof, Generalized gradient approximation made simple, *Phys. Rev. Lett.* **77**, 3865 (1996).
- [55] S. Smidstrup, D. Stradi, J. Wellendorff, P. A. Khomyakov, U. G. Vej-Hansen, M.-E. Lee, T. Ghosh, E. Jónsson, H. Jónsson, and K. Stokbro, First-principles Green's-function method for surface calculations: A pseudopotential localized basis set approach, *Phys. Rev. B* **96**, 195309 (2017).
- [56] S. Smidstrup, T. Markussen, P. Vanraeyveld, J. Wellendorff, J. Schneider, T. Gunst, B. Verstichel, D. Stradi, P. A. Khomyakov, U. G. Vej-Hansen, M.-E. Lee, S. T. Chill, F. Rasmussen, G. Penazzi, F. Corsetti, A. Ojanpera, K. Jensen, M. L. N. Palsgaard, U. Martinez, A. Blom, M. Brandbyge, and K. Stokbro, QuantumATK: an integrated platform of electronic and atomic-scale modelling tools, *J. Phys.: Condens. Matter* **32**, 015901 (2020).
- [57] M. J. van Setten, M. Giantomassi, E. Bousquet, M. J. Verstraete, D. R. Hamann, X. Gonze, and G. M. Rignanese, The PSEUDODOJO: Training and grading a 85 element optimized norm-conserving pseudopotential table, *Comp. Phys. Commun.* **226**, 39 (2018).
- [58] H. J. Monkhorst and J. D. Pack, Special points for Brillouin-zone integrations, *Phys. Rev. B* **13**, 5188 (1976).
- [59] A. I. Liechtenstein, M. I. Katsnelson, V. P. Antropov, and V. A. Gubanov, Local spin density functional approach to the theory of exchange interactions in ferromagnetic metals and alloys, *J. Magn. Magn. Mater.* **67**, 65 (1987).
- [60] J. M. Wills, M. Alouani, P. Andersson, A. Delin, O. Eriksson, and O. Grechnev, *Full-Potential Electronic Structure Method: Energy and Force Calculations With Density Functional and Dynamical Mean Field Theory*, Springer Series in Solid-State Sciences, Vol. 167 (Springer, 2010).
- [61] P. W. Anderson, Theory of magnetic exchange interactions: Exchange in insulators and semiconductors, in *Solid State Physics Volume 14*, edited by F. Seitz and D. Turnbull (Academic Press, New York, 1987) pp. 99–214.
- [62] E. Şaşıoğlu, L. M. Sandratskii, and P. Bruno, First-principles calculation of the intersublattice exchange interactions and curie temperatures of the full heusler alloys Ni_2MnX ($X = \text{Ga}, \text{In}, \text{Sn}, \text{Sb}$), *Phys. Rev. B* **70**, 024427 (2004).
- [63] S. Yamada, S. Kobayashi, F. Kuroda, K. Kudo, S. Abo, T. Fukushima, T. Oguchi, and K. Hamaya, Magnetic and transport properties of equiatomic quaternary heusler co-fevsi epitaxial films, *Phys. Rev. Mater.* **2**, 124403 (2018).
- [64] A. J. Garza and S. G. E., Predicting Band Gaps with Hybrid Density Functionals, *J. Phys. Chem. Lett.* **7**, 4165–4170 (2016).
- [65] J. Heyd, G. E. Scuseria, and M. Ernzerhof, Hybrid functionals based on a screened Coulomb potential, *J. Chem. Phys.* **118**, 8207 (2003).
- [66] J. Heyd, G. E. Scuseria, and M. Ernzerhof, Erratum: “Hybrid functionals based on a screened Coulomb potential” [J. Chem. Phys. 118, 8207 (2003)], *J. Chem. Phys.* **124**, 219906 (2006).
- [67] M. Tas, E. Şaşıoğlu, I. Galanakis, C. Friedrich, and S. Blügel, Quasiparticle band structure of the almost-gapless transition-metal-based Heusler semiconductors, *Phys. Rev. B* **93**, 195155 (2016).
- [68] P. Haas, F. Tran, and P. Blaha, Calculation of the lattice constant of solids with semilocal functionals, *Phys. Rev. B* **79**, 085104 (2009).
- [69] E. Şaşıoğlu, I. Galanakis, F. Friedrich, and Blügel, Ab initio calculation of the effective on-site Coulomb interaction parameters for half-metallic magnets, *Phys. Rev. B* **88**, 134402 (2013).
- [70] H. A. Dürr, G. van der Laan, D. Spanke, F. U. Hillebrecht, and B. N. B., Electron-correlation-induced magnetic order of ultrathin Mn films, *Phys. Rev. B* **56**, 8156 (1997).
- [71] M. Pajda, J. Kudrnovsky, I. Turek, V. Drchal, and P. Bruno, Ab initio calculations of exchange interactions, spin-wave stiffness constants, and Curie temperatures of Fe, Co, and Ni, *Phys. Rev. B* **64**, 174402 (2001).
- [72] E. Şaşıoğlu, L. Sandratskii, P. Bruno, and I. Galanakis, Exchange interactions and temperature dependence of magnetization in half-metallic Heusler alloys, *Phys. Rev. B* **72**, 184415 (2005).